Quantum-limited shot noise and quantum interference in graphene based Corbino disk

Grzegorz Rut and Adam Rycerz

Jagiellonian University, Reymonta 4, PL-30059 Krakow, Poland

grzegorz.rut@uj.edu.pl and rycerz@th.if.uj.edu.pl

Quantum Relativistic Corbino Effect

In the Corbino geometry a disk-shaped sample is surrounded from both interior and exterior sides with metallic leads (Fig. 1). Quite recently, an intriguing interference phenomenon was predicted theoretically for impurity-free Corbino disks both in mono (MLG) and bilayer graphene (BLG) [1, 2, 3]. At the Dirac point as well as on other Landau levels, the conductance exhibits oscillatory dependence on magnetic field due to the descrete spectrum of transmission modes. In general, nonzero conductance at high magnetic fields appears only in close vicinity of the Landau levels. Also, the QRCE was predicted in the linear response regime. Here we extend the analysis beyond the zero voltage limit in order to check how this affects this phenomenon.

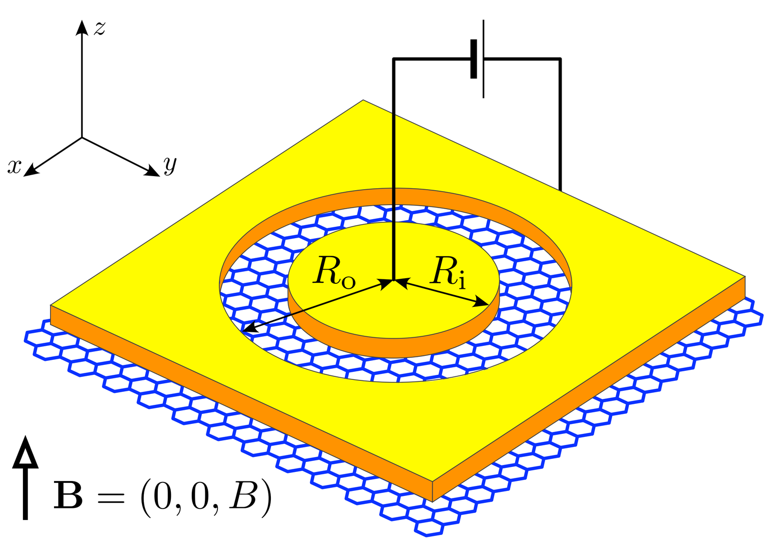

Figure 1: *The Corbino disk in graphene. The current is passed through the disk shaped area in a perpendicular magnetic field. The leads (yellow) are modeled with infinitely doped graphene.*

A clear view on this effect in MLG can be obtained by presenting G in the Fourier series

$$G = \frac{2g_0}{\mathcal{L}} + \sum_{m=1}^{\infty} G_m \cos\left(2\pi m \frac{\Phi_D}{\Phi_0}\right), \qquad (1)$$

with $G_m = (-1)^m g_0 (2\pi/\mathcal{L})^2 m \operatorname{csch}(\pi^2 m/\mathcal{L})$, where $g_0 = 4e^2/h$, $\Phi_D = \pi(R_o^2 - R_i^2)B$ is the flux piercing the ring, $\Phi_0 = 2(h/e)\mathcal{L}$, $\mathcal{L} = \ln(R_o/R_i)$, with inner R_i and outer R_o radii. The oscillations magnitude increase with radii ratio and exceed 10% of the average conductance for $R_o/R_i \geq 5$. Analogical oscillations are found for higher charge transfer cumulants as well.

In BLG oscillations amplitude at the Dirac point, depending on the size of the system, are up to two times larger than in MLG. On the other hand, at other Landau levels the oscillations are of the same magnitude for both materials, provided the valley degeneracy remains (see Fig. 2).

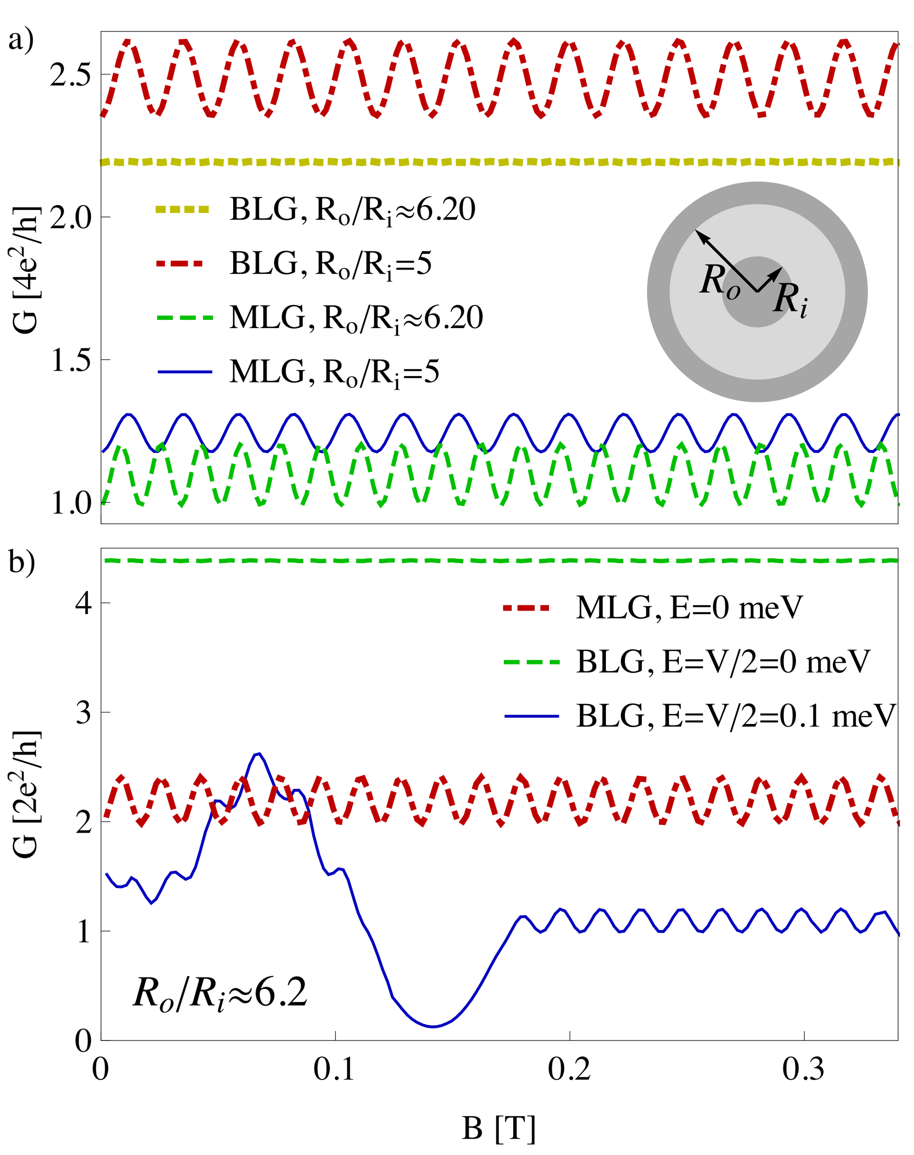

Figure 2: *Conductance of different graphene-based Corbino devices with the inner radius $R_i \simeq 80$ nmas a function of the magnetic field. (a) Magnetoconductance oscillations in mono- and bilayer disks at the Dirac point. (b) Conductance comparison with Corbino disk in BLG with nonzero electrostatic bias V between the layers at doping $V/2 = E$.*

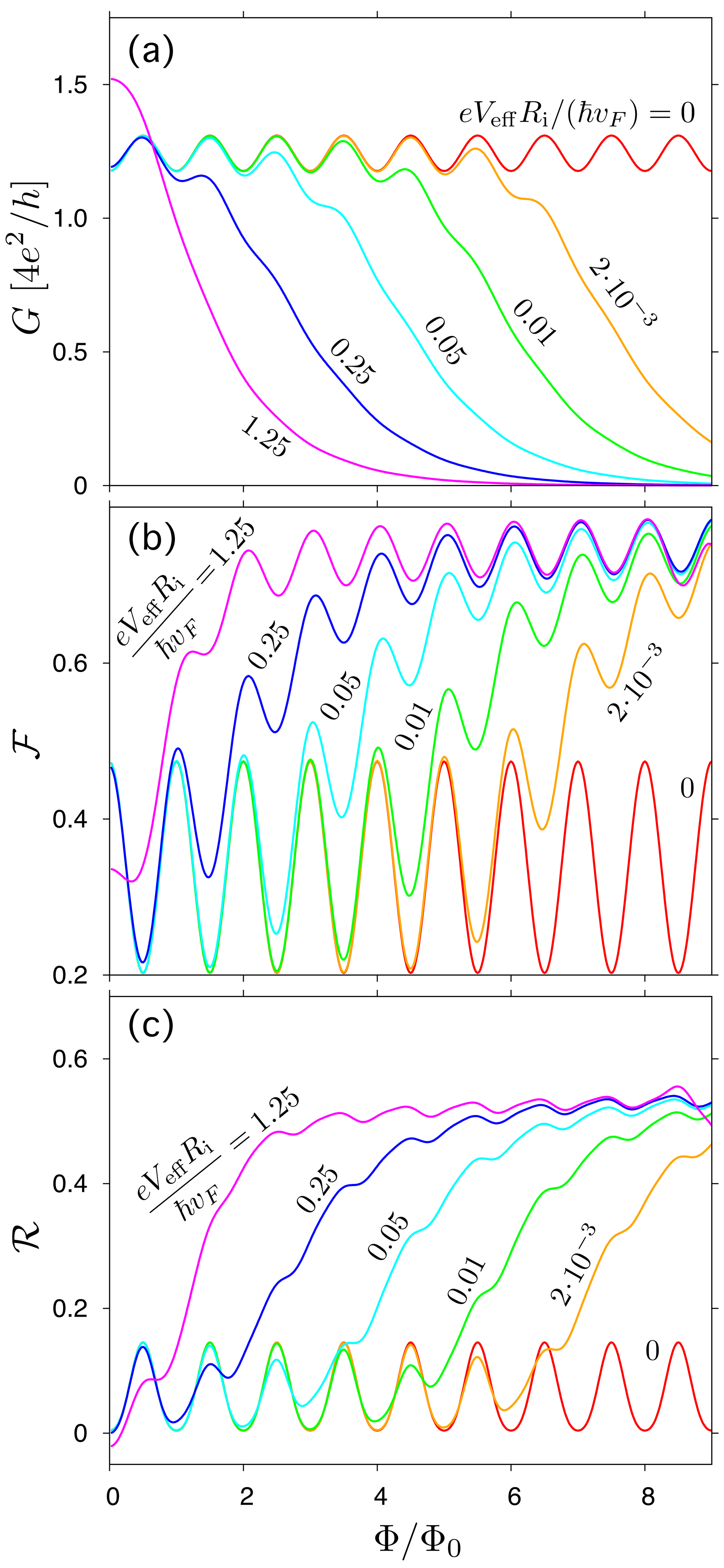

Figure 3: *Impact of increasing magnetic flux on the finite-voltage conductance (a), Fano factor (b) and $\mathcal{R}$-factor (c). The effective source-drain voltage $V_{\rm eff}$ is specified for each curve.*

Method

The conductance is derived within the Landauer-Bï¿½ttiker formalism with the aid of the Levitov formula

$$\ln\Lambda(\chi) \equiv \ln\langle \exp(i\chi Q/e)\rangle = \alpha \int_{\mu_0 - eV_{\rm eff}/2}^{\mu_0 + eV_{\rm eff}/2} d\varepsilon \sum_j \ln\left[1 + \left(e^{i\chi} - 1\right) T_j(\varepsilon)\right] \qquad (2)$$

where $\langle X \rangle$ denotes the expectation value of X, $\alpha = 4_{(\sigma,v)}\Delta t/h$, the factor $4_{(\sigma,v)}$ accounts for spin and valley degeneracies, Δt is a time interval, and we have assumed $V_{eff} > 0$ without loss of generality. The average charge $\langle Q \rangle$, as well as any charge-transfer cumulant $\langle\langle Q^m \rangle\rangle \equiv \langle (Q - \langle Q \rangle)^m \rangle$, may be obtained by subsequent differentiation of $\ln\Lambda(\chi)$ with respect to $i\chi$ at $\chi = 0$. In particular, the conductance

$$G(V_{\rm eff}) = \frac{\langle Q \rangle}{V_{\rm eff}\Delta t} = \frac{e}{V_{\rm eff}\Delta t} \left.\frac{\partial \ln\Lambda(\chi)}{\partial(i\chi)}\right|_{\chi=0} \equiv \frac{4_{(\sigma,v)}e^2}{h} \sum_j \langle T_j \rangle_{|\varepsilon - \mu_0| \leq eV_{\rm eff}/2}, \qquad (3)$$

where transmission probabilities $T_j(\varepsilon)$ are averaged over the energy interval $|\varepsilon - \mu_0| \leq eV_{\rm eff}/2$. Analogously,

$$\mathcal{F}(V_{\rm eff}) = \langle\langle Q^2 \rangle\rangle / \langle\langle Q^2 \rangle\rangle_{\rm Poisson}, \quad \mathcal{R}(V_{\rm eff}) = \langle\langle Q^3 \rangle\rangle / \langle\langle Q^3 \rangle\rangle_{\rm Poisson}, \qquad (4)$$

with $\langle\langle Q^m \rangle\rangle_{\rm Poisson}$ the value of m-th cumulant for the Poissonian limit $(T_j(\varepsilon) \ll 1)$, given by a generalized Schottky formula $\langle\langle Q^m \rangle\rangle_{\rm Poisson} = e^{m-1}\langle Q \rangle$.

Results

For the purpose of numerical demonstration, we choose $R_o/R_i = 5$, and focus on the vicinity of the Dirac point by setting $\mu_0 = 0$. The corresponding oscillation magnitudes, in the linear response limit, are

$$\Delta G(V_{\rm eff} \to 0) = 0.11\, G_{\rm diff}, \quad \Delta\mathcal{F}(V_{\rm eff} \to 0) = 0.27, \quad \Delta\mathcal{R}(V_{\rm eff} \to 0) = 0.14. \qquad (5)$$

A striking feature is the total lack of effects of both the radii ratio R_o/R_i and the source-dran voltage $V_{\rm eff}$ on limiting values $\overline{\mathcal{F}}_\infty \simeq 0.76$ and $\overline{\mathcal{R}}_\infty \simeq 0.55$ (in contrast, $\Delta\mathcal{F}_\infty$ and $\Delta\mathcal{R}_\infty$ strongly depends on R_o/R_i; see Figs. 3 and 4). The limiting values are expected to appear generically in graphene-based nanosystems at high magnetic fields and for finite source-drain voltages, similarly as pseudodiffusive shot noise ($\mathcal{F}_{\rm diff} = 1/3$ and $\mathcal{R}_{\rm diff} = 1/15$).

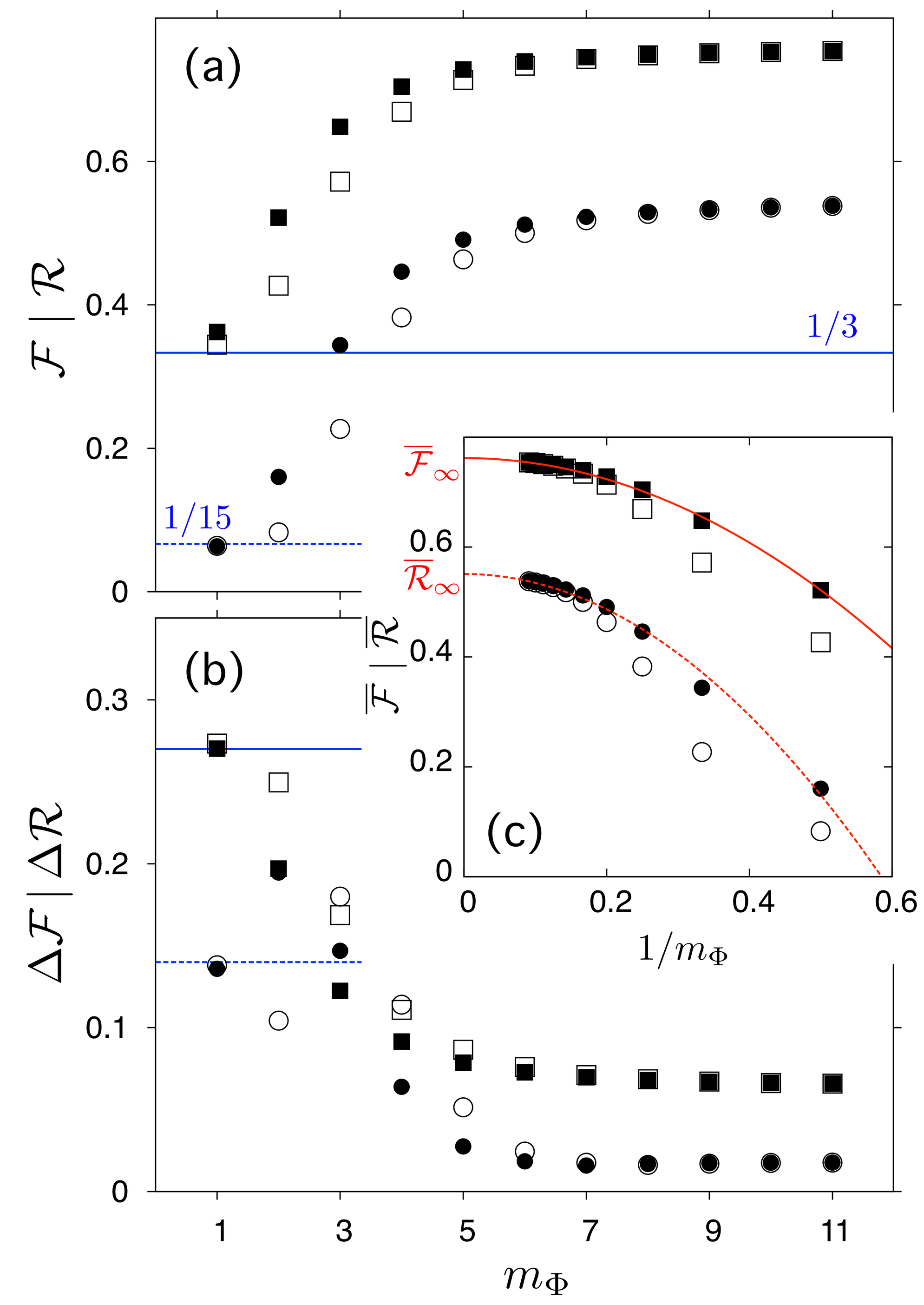

Figure 4: *Average values $\overline{X}$ (a) and oscillation amplitudes ΔX (b) with $X = \mathcal{F}$ (squares) and $X = \mathcal{R}$ (circles), calculated for several consecutive flux intervals. Open (or closed) symbols at each panel correspond to $eV_{\rm eff}R_i/\hbar v_F = .25$ (or .5). Lines depict the linear response values of $\mathcal{F}$ and $\mathcal{R}$. Panel (c) illustrates the scaling of $\overline{\mathcal{F}}$ and $\overline{\mathcal{R}}$ with $1/m_\Phi \to 0$.*

R_o/R_i	$\overline{\mathcal{F}}_\infty$	$\Delta\mathcal{F}_\infty$	$\overline{\mathcal{R}}_\infty$	$\Delta\mathcal{R}_\infty$
2.5	0.761(1)	0.0014(1)	0.552(3)	0.0064(2)
5.0	0.763(1)	0.061(1)	0.555(2)	0.017(1)
10	0.771(5)	0.191(2)	0.56(1)	0.170(2)

Table 1: *Limiting values of period-averaged $\overline{\mathcal{F}}$, $\overline{\mathcal{R}}$ and oscillation magnitudes $\Delta\mathcal{F}$, $\Delta\mathcal{R}$. Numbers in parentheses are standard deviations for the last digit.*

References

[1] A. Rycerz, Phys. Rev. B 81, 121405 (R) (2010).

[2] M.I. Katsnelson, Europhys. Lett. 89, 17001 (2010).

[3] G. Rut and A. Rycerz, arXiv:1405.4908

[4] G. Rut and A. Rycerz, arXiv:1401.7247

The work was realised in the Project TEAM awarded to our group by the Foundation for Polish Science (FNP) for the years 2011-2014.

EUROPEAN UNION EUROPEAN REGIONAL DEVELOPMENT FUND

FNP Foundation for Polish Science

INNOVATIVE ECONOMY NATIONAL COHESION STRATEGY